

# Towards Differential Handling of Various Blur Regions for Accurate Image Deblurring

Hu Gao  
Beijing Normal University  
Beijing, China  
gao\_h@mail.bnu.edu.cn

Depeng Dang  
Beijing Normal University  
Beijing, China  
ddepeng@bnu.edu.cn

## Abstract

Image deblurring aims to restore high-quality images by removing undesired degradation. Although existing methods have yielded promising results, they either overlook the varying degrees of degradation across different regions of the blurred image. In this paper, we propose a differential handling network (DHNet) to perform differential processing for different blur regions. Specifically, we design a Volterra block (VBlock) to incorporate nonlinear characteristics into the deblurring network, enabling it to map complex input-output relationships without relying on nonlinear activation functions. To enable the model to adaptively address varying degradation degrees in blurred regions, we devise the degradation degree recognition expert module (DDRE). This module initially incorporates prior knowledge from a well-trained model to estimate spatially variable blur information. Consequently, the router can map the learned degradation representation and allocate weights to experts according to both the degree of degradation and the size of the regions. Comprehensive experimental results show that DHNet effectively surpasses state-of-the-art (SOTA) methods on both synthetic and real-world datasets.

## 1. Introduction

Image deblurring seeks to restore high-quality images from these blur versions. Due to the ill-posed nature, traditional method [20] attempts to tackle it by imposing various priors to limit the solution space. However, creating such priors is difficult and often lacks generalizability, making them impractical for real-world applications.

In recent years, a variety of Convolutional Neural Networks (CNNs) [7, 8, 10, 16, 42] have been developed for image deblurring. The fundamental component of a CNN is a convolutional layer followed by an activation function. The convolution operation ensures local connectivity and

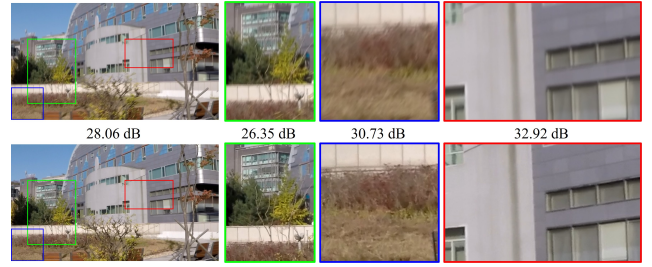


Figure 1. Varying degrees of degradation across different regions. The top row is the blurred image and the bottom row is the sharp image.

translational invariance, while the activation function adds non-linearity to the network. However, CNNs face inherent limitations, such as local receptive fields and a lack of dependence on input content, which restrict their ability to eliminate long-range blur degradation perturbation. To overcome such limitations, Transformers [15, 22, 30, 43] have been introduced in image deblurring. They leverage the adaptive weights of the self-attention mechanism and excel at capturing global dependencies, demonstrating superior performance compared to CNN-based approaches.

While the aforementioned methods have demonstrated strong performance in image deblurring, they have two key drawbacks: (1) they approximate nonlinear function properties by stacking numerous nonlinear activation functions, and (2) they overlook the varying degrees of degradation across different blur regions of the image. As shown in Figure 1, the degradation in a blurred image varies across different regions. The areas highlighted by the green box are more severely blurred than those marked by the red box.

To tackle the first drawback, NAFNet [2] argues that high complexity is unnecessary and proposes a simpler baseline that employs element-wise multiplication instead of nonlinear activation functions, achieving better results with lower computational resources. However, this approach inevitably sacrifices the ability to map complex input-output relation-

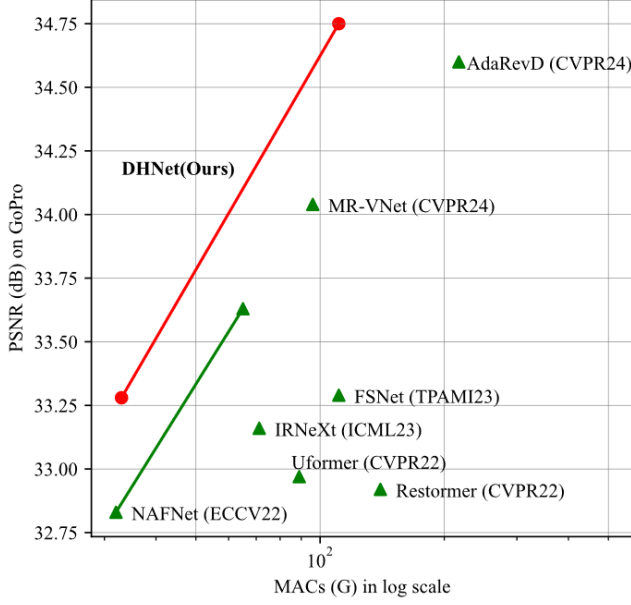


Figure 2. Computational cost vs. PSNR of models on the GoPro dataset [29]. Our DHNet achieve the SOTA performance with up to 48.9% of cost reduction.

ships, making it difficult to manage more intricate scenes. To address the second issue, AdaRevD [27] introduces a classifier to assess the degradation degree of image patches. However, this method relies on a limited number of predefined categories and a fixed blur patch size<sup>1</sup> to specify the degree of degradation, which diminishes its effectiveness in adaptively managing different degrees of degradation across various sizes of blurred patches.

Based on the analyses presented above, a natural question arises: Is it feasible to devise a network that effectively performs differential processing for different blur regions with less nonlinear activation function? In pursuit of this objective, we propose DHNet for efficient image deblurring, incorporating several key components. 1) We design a Volterra block (VBlock) to investigate non-linearity within the network. VBlock avoids using traditional nonlinear activation functions and instead employs Volterra kernel to enhance linear convolution by facilitating interactions between image pixels. This approach approximates non-linearity without the computational overhead associated with stacking numerous nonlinear functions to map complex input-output relationships. 2) To adaptively identify degradation degrees across varying sizes of blur regions, we propose a degradation degree recognition expert module (DDRE). DDRE first integrates prior knowledge

<sup>1</sup> AdaRevD groups the patches into six degradation degrees based on the PSNR between the blurred patch and the sharp patch, and then uses a relatively large patch size of 384 x 384 to classify the degradation degree of each blurred patch.

from a well-trained model to estimate the spatially variable blur information. This enables the router to map the learned degradation representation and assign weights to experts based on both the degree of degradation and the size of the regions. We conduct extensive experiments to validate the effectiveness of the proposed networks, demonstrating their remarkable performance advantage over state-of-the-art approaches. As illustrated in Figure 2, our DHNet model achieves SOTA performance while requiring less computational cost compared to existing methods.

The main contributions are summarized as follows:

1. We propose an efficient and effective framework for image deblurring, called DHNet, which excels at differentially handling various blur regions while maintaining lower computational costs.
2. We design a Volterra block (VBlock) to investigate non-linearity within the network, avoiding the previous operation of stacking numerous nonlinear functions to map complex input-output relationships.
3. We devise a degradation degree recognition expert module (DDRE), enabling the model adaptively deal with the different degradation degrees of the degraded region.
4. Extensive experiments demonstrate that the proposed DHNet achieves promising performance compared to state-of-the-art methods across synthetic and real-world benchmark datasets.

## 2. Related Work

### 2.1. Image Deblurring

The ill-posed nature of image deblurring leads many conventional approaches [12, 20] to rely on hand-crafted priors to limit the possible solutions. Although these priors can assist in blur removal, they often struggle to accurately model the degradation process and often lack generalization.

Rather than manually designing image priors, many methods focus on developing various deep CNNs [2, 6–10, 17, 27, 33, 42, 44] to tackle image deblurring. MPRNet [42] presents a multi-stage progressive approach that improves the exploration of spatial details and contextual information. MIRNet-V2 [44] employs a multi-scale architecture that maintains spatially precise representations while also capturing complementary contextual insights. CGNet [17] integrates a global context extractor to effectively gather global contextual information. IRNeXt [7] rethinks CNN design and introduces an efficient network. FSNet [10] utilizes multi-branch and content-aware modules to dynamically select the most informative components. MR-VNet [33] proposes a novel architecture that leverages Volterra layers for both image and video restoration. Nonetheless, the inherent characteristics of convolutional operations, such as local receptive fields, limit the models’ ability to effectively address long-range degrada-

tion disturbances.

To tackle these limitations, Transformers [11, 22, 24, 25, 30, 36, 38, 43, 45] have been utilized in image deblurring. They effectively capture global dependencies through the adaptive weights of the self-attention mechanism, outperforming CNN-based methods. However, the quadratic time complexity of the self-attention mechanism with respect to input size increases the computational burden. To mitigate this issue, Uformer [38], SwinIR [24], and U<sup>2</sup>former [15] implement self-attention using a window-based approach. In contrast, Restormer [43], MRLPFNet [11], and Deblur-DiNAT [25] compute self-attention across channels rather than in the spatial dimension, achieving linear complexity in relation to input size. Additionally, FFTformer [22] leverages frequency domain properties to estimate scaled dot-product attention.

While the aforementioned methods have two main drawbacks: (1) they approximate nonlinear functions by stacking many nonlinear activation functions, and (2) they fail to account for the varying degrees of degradation in different blur regions. Although NAFNet [2] uses element-wise multiplication instead of nonlinear activation functions, it struggles with more complex scenes. AdaRevD [27] introduces a classifier to assess the degradation degree of image patches, but it relies on a limited number of predefined categories and a fixed patch size, lacking adaptive flexibility. In this paper, we propose a differential handling network that incorporates two key components: the Volterra block (VBlock) and the degradation degree recognition expert module (DDRE). This network achieves nonlinear properties with fewer nonlinear activation functions while adaptively handling varying degradation degrees in blur regions of different sizes.

## 2.2. Volterra Series

The Volterra series is a model for nonlinear behavior that effectively captures "memory" effects [37]. With its capability to learn nonlinear functions, Volterra Filters have been applied in deep learning [1, 32, 33, 46]. To enhance non-linearity and complement traditional activation functions, [46] introduces a single layer of Volterra kernel-based convolutions followed by standard CNN layers. VNNs [32] proposes a cascaded approach of Volterra Filtering to significantly reduce the number of parameters. VolterraNet [1] presents a novel higher-order Volterra convolutional neural network designed for data represented as samples of functions on Riemannian homogeneous spaces. MR-VNet [33] uses Volterra layers to effectively introduce nonlinearities into the image restoration process. However, in MR-VNet, only the second-order nonlinearity is captured, while the first-order nonlinearity is overlooked. This results in reduced attention to local features and a higher risk of gradient explosion. In this paper, we design a VBlock that

addresses these issues and approximates nonlinearity without the computational burden of stacking multiple nonlinear functions.

## 2.3. Mixture of Experts

Mixture of Experts (MoE) [19] consists of multiple experts and a routing network that combines their outputs using a weighted strategy. Its main goal is to enhance model performance by scaling up parameters while maintaining computational efficiency [3–5, 14, 28, 34, 40, 41]. HCTFFN [5] leverages MoE to highlight features related to spatially varying rain distribution. DRSformer [4] incorporates an MoE feature compensator for a unified exploration of joint data and content sparsity. DAN-Net [40] employs MoE to extract degradation information from each input image. Lifelong-MoE [3] uses pre-trained experts and gates to retain prior knowledge. In contrast to the methods mentioned above, we incorporate prior knowledge into DDRE from a well-trained model to estimate spatially variable blur information. This allows the router to adaptively allocate weights to different experts, enabling them to address the varying degradation degrees presented by different blur regions.

## 3. Method

In this section, we begin with an overview of the entire DHNet pipeline. Following that, we delve into the details of the proposed differential handling block (DHBlock), which serves as the fundamental building unit of our method. This block primarily consists of two key components: the Volterra block (VBlock) and the degradation degree recognition expert module (DDRE).

### 3.1. Overall Pipeline

Our proposed DHNet, depicted in Figure 3, employs a hierarchical encoder-decoder architecture to facilitate effective hierarchical representation learning. Each encoder-decoder includes a DHBlock, which consists of  $N_{i \in [1, \dots, 9]}$  VBlocks and a degradation degree recognition expert module (DDRE). Given a degraded image  $\mathbf{I} \in \mathbb{R}^{H \times W \times 3}$ , DHNet first applies convolution to extract shallow features  $\mathbf{F}_s \in \mathbb{R}^{H \times W \times C}$  (where  $H$ ,  $W$ , and  $C$  represent the height, width, and number of channels of the feature map, respectively). These shallow features pass through a four-scale encoder sub-network, where the resolution is progressively reduced while the number of channels increases. The resulting in-depth features then move to a middle block, and the deepest features are processed by a four-scale decoder, which gradually restores them to their original size. Finally, we apply convolution to the refined features to generate a residual image  $\mathbf{X} \in \mathbb{R}^{H \times W \times 3}$ . This residual image is added to the degraded image to produce the restored image:  $\hat{\mathbf{I}} = \mathbf{X} + \mathbf{I}$ .

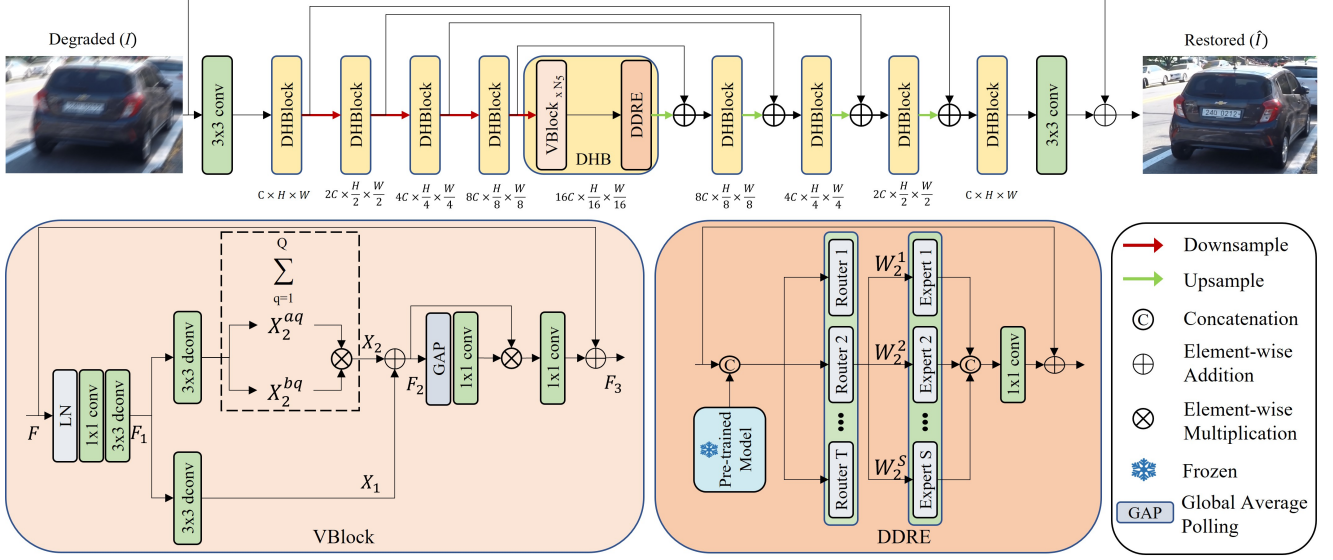


Figure 3. The overall architecture of the proposed differential handling network (DHNet) for image deblurring mainly consists of the differential handling block (DHBlock), which includes the Volterra block (VBlock) and the degradation degree recognition expert module (DDRE). DDRE is shown in the one-router case for clarity.

### 3.2. Differential Handling Block

While existing image deblurring methods have demonstrated commendable performance, they often rely on stacking numerous nonlinear activation functions to approximate nonlinear properties, neglecting the varying degradation degrees across different blurred regions. To address this issue, we design the differential handling block (DHBlock) as a feature extractor, enabling differential processing of diverse blur regions and utilizing Volterra kernel to capture complex input-output relationships. Formally, given the input features at the  $(l-1)_{th}$  block  $X_{l-1}$ , the procedures of DHBlock can be defined as:

$$\begin{aligned} X'_l &= VBlock_{N_i}(\dots(VBlock_1(X_{l-1}))) \dots \\ X_l &= DDRE(X'_l) \end{aligned} \quad (1)$$

where  $N_i$  represents the number of VBlocks in the DHBlock, while  $X'_l$  and  $X_l$  denote the outputs from the  $N_i$  Volterra blocks (VBlocks) and the degradation degree recognition expert module (DDRE), which are detailed below.

### 3.3. Volterra Block

The strong performance and versatility of deep learning-based image deblurring models [10, 27] can be attributed to their nature as universal approximators. They achieve this by stacking numerous nonlinear activation functions, allowing them to fit any nonlinear function. In order to reduce the system complexity caused by an excess of nonlinear activation functions, we design a Volterra block (VBlock) that

utilizes the Volterra kernel to explore non-linearity within the network. Instead of relying on traditional nonlinear activation functions, VBlock employs higher-order convolutions to enhance linear convolution by enabling interactions between image pixels. As shown in Figure 3, unlike MRVNet [33], which treats the Volterra filter as a complete block, our VBlock incorporates it as part of a block. The VBlock first captures local features using LN, 1x1, and 3x3 convolutions before entering the Volterra filter, and then applies two 3x3 convolutions for each order branch. Specifically, our VBlock takes an input tensor  $F$ , first applies layer normalization (LN), and then encodes channel-wise context by utilizing 1x1 convolutions followed by 3x3 depth-wise convolutions to obtain the feature  $F_1$  as follows:

$$F_1 = W_d^0 W_p^0 LN(F) \quad (2)$$

where  $W_p^{(\cdot)}$  denotes the  $1 \times 1$  point-wise convolution, and  $W_d^{(\cdot)}$  represents the  $3 \times 3$  depth-wise convolution.

The resulting feature  $F_1$  is then processed by the second-order Volterra kernel to capture complex input-output relationships through interactions between image pixels. In this paper, we compute the second-order Volterra kernel as a product of traditional correlation operations. This representation can achieve an approximation error with arbitrary precision. Moreover, the separability assumption of the kernels enables efficient computation, which is especially ad-



vantageous in network settings. The process is as follows:

$$\begin{aligned}
F_2 &= X_1 \oplus X_2 \\
&= W_d^1 F_1 \oplus \left( \sum_{q=1}^Q X_2^{aq} \otimes X_2^{bq} \right) \\
&= W_d^1 F_1 \oplus \left( \sum_{q=1}^Q W_d^{2aq} F_1 \otimes W_d^{2bq} F_1 \right)
\end{aligned} \tag{3}$$

where  $W_d^{2aq}$  and  $W_d^{2bq}$  are learnable weight matrices,  $Q$  represents the desired rank of approximation.

**Theorem 1.** Any continuous function can be approximated using a Volterra kernel.

**Proof.** Any continuous nonlinear function can be approximated by a polynomial. Similarly to VNNs [32], using a Taylor expansion at  $x_0$ , the nonlinear function  $\sigma(\cdot)$  can be represented as:

$$\begin{aligned}
\sigma_t(x) &= f(x_0) + \dots + \frac{f^{(n)}(x_0)}{n!} (x - x_0)^n + R_n(x) \\
&= \alpha_0 + \alpha_1 x + \dots + \alpha_n x^n + R_n(x)
\end{aligned} \tag{4}$$

For a memoryless higher-order Volterra kernel, it can be formulated as:

$$\sigma_v(x) = h_0 + h_1 x + \dots + h_n x^n \tag{5}$$

where  $h_n$  represents the  $n_{th}$  order weight, which is learned during the training process. The function  $\sigma_v(x)$  can be considered an  $n_{th}$  order approximation of  $\sigma_t(x)$ , with the error defined as:

$$error = (\alpha_0 - h_0) + \dots + (\alpha_n - h_n) x^n + R_n(x) \tag{6}$$

For a finite polynomial, the absolute error of the expansion can be quantitatively expressed using the Taylor Remainder as follows:

$$|error| \leq R_n(x) = \frac{f^{(n+1)}(\xi)}{(n+1)!} (x - x_0)^{n+1} \tag{7}$$

where  $\xi \in (x_0, x)$ . Due to the complexity of higher-order Volterra kernels, this paper utilizes a cascade of second-order Volterra kernels to approximate the higher-order behavior (refer to supplementary material for the proof).

**Theorem 2.** A Volterra kernel provide more adaptive representation than that possible by activation functions.

**Proof.** For nonlinear activation functions such as ReLU, sigmoid, and tanh, the coefficients  $\alpha_n$  in their Taylor expansions are predetermined<sup>2</sup>. Specifically, a sigmoid activation can be approximated as:

$$\sigma_s(x) = \frac{1}{1 + e^{-x}} = \frac{1}{2} + \frac{1}{4}x - \frac{1}{48}x^3 + \dots \tag{8}$$

<sup>2</sup>The term "predetermined" refers to a fixed value that remains constant.

The expansion coefficient  $h_n$  of the Volterra kernel can be continuously adjusted and learned during training, allowing for greater adaptability and more precise mapping of complex scenes. As a result, the feature  $F_2$  in Eq. 3 exhibits nonlinear characteristics and offers greater flexibility compared to features obtained through nonlinear activation functions (e.g. sigmoid). Finally, we apply channel attention to  $F_2$  to obtain the final output features  $F_3$  of VBlock as follows:

$$F_3 = W_p^2(F_2 \otimes (W_p^1 GAP(F_2))) \oplus F \tag{9}$$

### 3.4. Degradation Degree Recognition Expert Module

While existing image deblurring methods [33] have demonstrated strong performance, they overlook the inconsistency in the degradation degree across different regions. As illustrated in Figure 1, the degree of degradation in a blurred image can differ significantly between areas. Thus, it is clearly unreasonable for these methods to assume that all degraded areas share the same degree of degradation. In contrast to AdaRevD [27], which relies on a limited set of predefined categories and a fixed blur patch size, DDRE first incorporates prior knowledge from a well-trained model to estimate the spatially variable blur information. This enables DDRE to allow the router to map the learned degradation representation and assign weights to experts according to both the degree of degradation and the size of the regions.

Different from the conventional mixture of experts [3, 41] that select only one router and a subset of experts for each router, our DDRE utilizes all routing paths, dynamically assigning weights to each expert along every router. Each expert comprises convolutions with varying receptive field sizes, allowing for the identification of degraded regions of different sizes. For simplicity, Figure 3 illustrates a scenario with just one router. Given an input feature map  $F_4$ , we first integrate prior knowledge from a well-trained model and keeps it frozen during training for lower memory consumption as:

$$F_5 = W_p^3[F_4, P] \tag{10}$$

where  $P$  is the prior knowledge and  $[\cdot]$  denotes the concatenation. The feature map  $F_5$  that aggregate the degradation information is then input to each router, which assigns weights to each expert as follows:

$$F_6 = [W_j^k E_k(F_5)] \tag{11}$$

where  $W_j^k$  represents the learnable weight coefficient assigned by each router  $j \in \{1, 2, \dots, T\}$  to each expert  $k \in \{1, 2, \dots, S\}$ , and  $E$  is the expert operations. Finally, the output of the DDRE is calculated by:

$$F_7 = W_p^4 F_6 \oplus F_4 \tag{12}$$

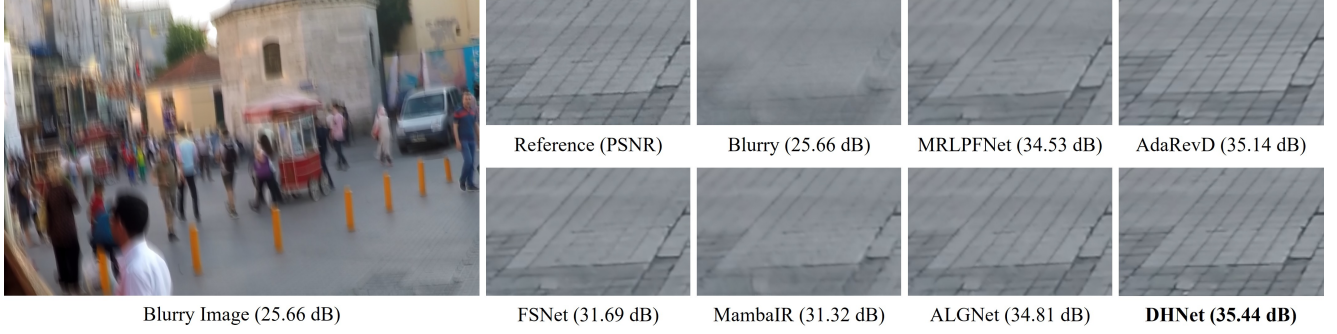


Figure 4. Image motion deblurring comparisons on the GoPro dataset [29]. Our DHNet recovers image with clearer details.

With this design, DDRE can adaptively handle varying degradation degrees across different sizes of degraded regions.

## 4. Experiments

In this section, we outline the experimental settings and present both qualitative and quantitative comparisons between DHNet and other state-of-the-art methods. We then conduct ablation studies to highlight the effectiveness of our approach. The best and second-best results in the tables are indicated in **bold** and underlined formats, respectively.

### 4.1. Experimental Settings

#### 4.1.1. Training details

We train separate models for different tasks, and unless otherwise specified, the following parameters are utilized. In our model,  $N_{i \in [1,2,3,4,5,6,7,8,9]}$  are set to  $\{1, 1, 1, 28, 1, 1, 1, 1, 1\}$ . In terms of VBlock, we set  $Q = 4$  (Eq. 3). In terms of DDRE, we set  $S = 5$  for the number of experts and  $T = 4$  for the number of routers. We use the Adam optimizer [21] with parameters  $\beta_1 = 0.9$  and  $\beta_2 = 0.999$ . The initial learning rate is set to  $5 \times 10^{-4}$  and gradually reduced to  $1 \times 10^{-6}$  using the cosine annealing strategy [26]. The batch size is chosen as 32, and patches of size  $256 \times 256$  are extracted from training images. Data augmentation includes both horizontal and vertical flips. Given the high complexity of image motion deblurring, we set the number of channels to 32 for DHNet and 64 for DHNet-B. In DHNet, we do not use a pre-trained model in the DDRE, whereas DHNet-B utilizes UFPNet [13].

#### 4.1.2. Datasets

We validate the effectiveness of our method using the GoPro dataset [29], which consists of 2,103 training image pairs and 1,111 evaluation pairs, in line with recent approaches [10]. To evaluate the generalizability of our model, we apply the GoPro-trained model to the HIDE [35] dataset, containing 2,025 images specifically designed for human-aware motion deblurring. Both the GoPro and HIDE

Table 1. Quantitative evaluations of the proposed approach against state-of-the-art motion deblurring methods. Our DHNet and DHNet-B are trained only on the GoPro dataset.

Methods	GoPro		HIDE	
	PSNR $\uparrow$	SSIM $\uparrow$	PSNR $\uparrow$	SSIM $\uparrow$
MPRNet [42]	32.66	0.959	30.96	0.939
Restormer [43]	32.92	0.961	31.22	0.942
Uformer [38]	32.97	0.967	30.83	0.952
NAFNet-32 [2]	32.83	0.960	-	-
NAFNet-64 [2]	33.62	0.967	-	-
IRNeXt [7]	33.16	0.962	-	-
SFNet [8]	33.27	0.963	31.10	0.941
DeepRFT+ [39]	33.23	0.963	31.66	0.946
UFPNet [13]	34.06	0.968	31.74	0.947
MRLPFNet [11]	34.01	0.968	31.63	0.947
MambaIR [18]	33.21	0.962	31.01	0.939
ALGNet-B [16]	34.05	0.969	31.68	<u>0.952</u>
MR-VNet [33]	34.04	0.969	31.54	0.943
FSNet [10]	33.29	0.963	31.05	0.941
AdaRevD-B [27]	34.50	0.971	32.26	<u>0.952</u>
AdaRevD-L [27]	34.60	<u>0.972</u>	<u>32.35</u>	<b>0.953</b>
<b>DHNet(Ours)</b>	33.28	0.964	31.75	0.948
<b>DHNet-B(Ours)</b>	<b>34.75</b>	<b>0.973</b>	<b>32.37</b>	<b>0.953</b>

datasets are synthetically generated. Additionally, we assess our method’s performance on real-world images using the RealBlur [31] dataset, which contains 3,758 training image pairs and 980 testing pairs, divided into two subsets: RealBlur-J and RealBlur-R.

### 4.2. Experimental Results

#### 4.2.1. Evaluations on the synthetic dataset.

We present the performance of various image deblurring methods on the synthetic GoPro [29] and HIDE [35] datasets in Table 1. Overall, our DHNet outperforms competing approaches, yielding higher-quality images with superior PSNR and SSIM values. Specifically, compared to our baseline model, NAFNet [2], DHNet improves performance by 0.45 dB and 1.13 dB with 32 and 64 channels,

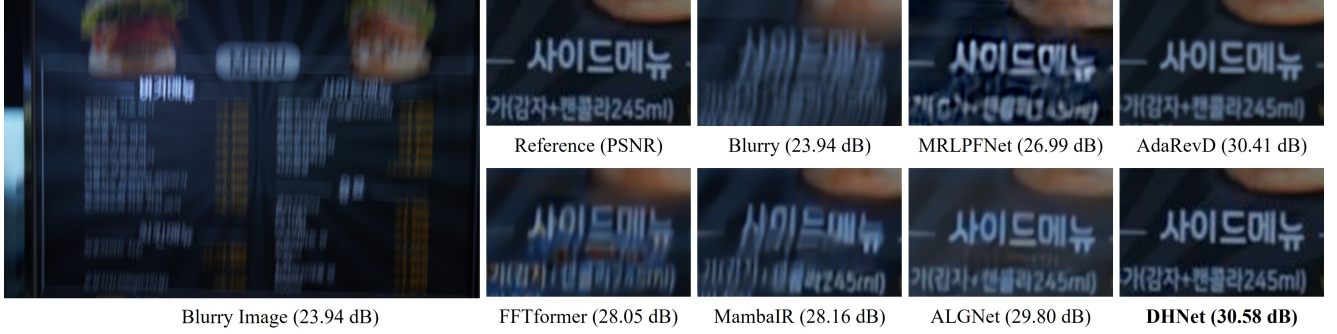


Figure 5. Image motion deblurring comparisons on the RealBlur dataset [31]. Our DHNet recovers perceptually faithful images.

Table 2. Quantitative evaluations of the proposed approach against state-of-the-art methods on the real-word dataset RealBlur [31].

Methods	RealBlur-R		RealBlur-J	
	PSNR $\uparrow$	SSIM $\uparrow$	PSNR $\uparrow$	SSIM $\uparrow$
DeblurGAN-v2 [23]	36.44	0.935	29.69	0.870
MPRNet [42]	39.31	0.972	31.76	0.922
DeepRFT+ [39]	39.84	0.972	32.19	0.931
Stripformer [36]	39.84	0.975	32.48	0.929
FFTformer [22]	40.11	0.973	32.62	0.932
UFPNet [13]	40.61	0.974	33.35	0.934
MambaIR [18]	39.92	0.972	32.44	0.928
ALGNet [16]	41.16	0.981	32.94	0.946
MR-VNet [33]	40.23	0.977	32.71	0.941
AdaRevD-B [27]	41.09	0.978	33.84	0.943
AdaRevD-L [27]	41.19	0.979	33.96	0.944
<b>DHNet(Ours)</b>	<b>41.30</b>	<b>0.984</b>	33.78	0.952
<b>DHNet-B(Ours)</b>	<b>41.33</b>	<b>0.983</b>	<b>34.28</b>	<b>0.953</b>

respectively. In comparison to the previous best method, AdaRevD-L [27], our DHNet-B shows an improvement of 0.15 dB on the GoPro [29] dataset. Notably, although our model was trained exclusively on the GoPro [29] dataset, it still achieves state-of-the-art results (32.37 dB in PSNR) on the HIDE [35] dataset, demonstrating its excellent generalization capability. Furthermore, Figure 2 shows that DHNet not only achieves state-of-the-art performance but also reduces computational costs. The performance continues to improve with an increase in model size, highlighting the scalability of our approach. Finally, Figure 4 presents deblurred images from the evaluation methods, where our model produces more visually pleasing results.

#### 4.2.2. Evaluations on the real-world dataset.

In addition to evaluating on synthetic datasets, we further assess the performance of our DHNet on real-world images from the RealBlur dataset [31]. As shown in Table 2, our method produces deblurred images with superior PSNR and SSIM scores. Specifically, compared to the previous best method, AdaRevD-L [27], our approach achieves improvements of 0.14 dB and 0.32 dB on the RealBlur-R and

Table 3. Ablation study on individual components of the proposed DHNet.

Net	VBlock	DDRE	PSNR	$\Delta$ PSNR
(a)			33.62	-
(b)	✓		34.05	+0.43
(c)		✓	34.32	+0.70
(d)	✓	✓	34.75	+1.13

RealBlur-J datasets, respectively. Figure 5 demonstrates that DHNet produces clearer images with finer details and structures, outperforming the competing methods.

### 4.3. Ablation Studies

In this section, we first demonstrate the effectiveness of the proposed modules and then investigate the effects of different designs for each module.

#### 4.3.1. Effects of Individual Components

To evaluate the effectiveness of each module, we use NAFNet [2] as our baseline model and subsequently replace or add the modules we have designed. As shown in Table 3(a), the baseline achieves 33.62 dB PSNR. Each module combination leads to a corresponding performance improvement. Specifically, replacing NAFBlock [2] with our VBlock enhances the performance by 0.43 dB (Table 3(b)). Adding the DDRE module to the original NAFNet [2] can significantly boost the model’s performance from 33.62 dB to 34.32 dB (Table 3(c)). When all modules are combined (Table 3(d)), our model achieves a 1.13 dB improvement over the original baseline.

#### 4.3.2. Design Choices for VBlock

VBlock facilitates the generation of nonlinear interactions through the interactions between image pixels. To evaluate the effectiveness of VBlock, we first use SG [2] to replace the Volterra kernel and then examine the impact of varying the kernel rank. As shown in Table 7, the SG [2] achieves a PSNR of 34.12 dB, and performance improves



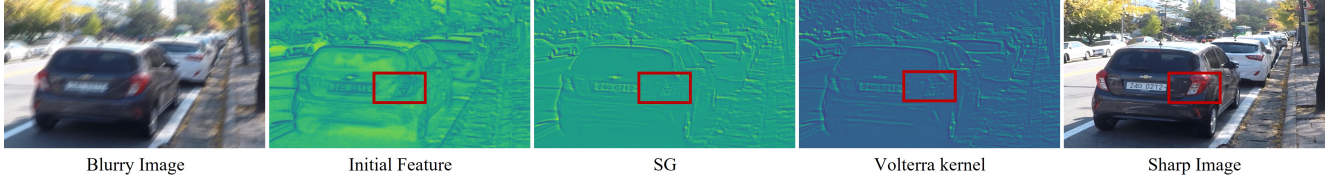


Figure 6. Effect of the proposed VBlock. Zoom in for the best view.

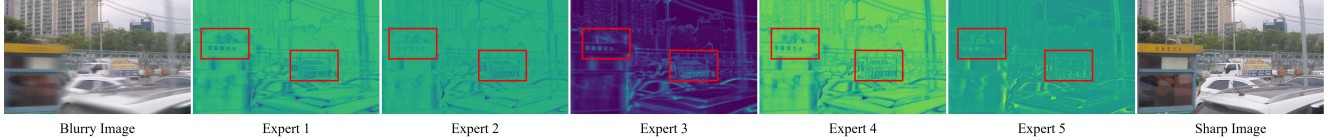


Figure 7. Effect of the proposed DDRE. Zoom in for the best view.

Table 4. Results of alternatives to VBlock.

Net	SG [2]	Volterra	Q	PSNR	$\Delta$ PSNR	MACs(G)
(a)	✓		0	34.12	-	106
(b)		✓	1	34.25	+0.13	107
(c)		✓	2	34.42	+0.30	109
(d)		✓	4	34.75	+0.63	111
(e)		✓	8	34.76	+0.64	119

when we implement our Volterra kernel. We further visualize the feature maps in Figure 6 to highlight the advantages of our Volterra kernel compared to SG [2]. The results clearly demonstrate that features obtained with the Volterra kernel are more detailed (as indicated by the red box) and better suited for handling complex scenes. Additionally, we analyze the effect of the  $Q$  value on the performance. As we increase the rank  $Q$ , performance consistently improves, but this also increases system complexity. To achieve a balance between efficiency and performance, we choose an experimental setting with  $Q = 4$ .

#### 4.3.3. Design Choices for DDRE

To evaluate the effectiveness of DDRE, we conduct experiments with various model variants, as shown in Table 5. When we introduce experts (Table 5 (b)) into the baseline model (Table 5 (a)), performance improves from 34.05 to 34.26, highlighting the model’s capability to address degradation in a differentiated manner. Further enhancement occurs when we incorporate external degradation pattern knowledge, leading to even greater performance gains (Table 5 (c) and (d)). Additionally, we observe that different pre-trained models (NAFNet [2], UFPNet [13]) yield varying performance outcomes. We also investigate the impact of the number of routers and experts on the experimental results. Our findings indicate that the combination of  $S = 5$  and  $T = 4$  (Table 5 (d)) yields the best results. A smaller number (Table 5 (e) (g)) fails to adequately identify the

Table 5. Results of alternatives to DDRE, where  $S$  and  $T$  denote the number of experts and routers, respectively.

Net	Pre-trained		T	S	PSNR	$\Delta$ PSNR
	NAFNet [2]	UFPNet [13]				
(a)			0	0	34.05	-
(b)			4	5	34.26	+0.21
(c)	✓		4	5	34.47	+0.35
(d)		✓	4	5	34.75	+0.70
(e)		✓	4	3	34.56	+0.51
(f)		✓	4	8	34.61	+0.56
(g)		✓	2	5	34.51	+0.46
(h)		✓	6	5	34.57	+0.52

degradation degree. While an excessive number (Table 5 (f) (h)) tends to focus on the severely degraded regions, and the lightly degraded regions will receive relatively less attention, ultimately hindering their restoration. To further demonstrate the effectiveness of our DDRE module, we visualize the features of a routing path weighted over all experts, as shown in Figure 7. It is clear that each expert handles the inconsistent degradation region as well as the degree of restored degradation.

## 5. Conclusion

In this paper, we propose a differential handling network (DHNet) aimed at accurately deblurring images by processing different blur regions. Specifically, we design a DHBlock consisting of VBlock and DDRE. The VBlock utilizes the Volterra kernel to explore non-linearity within the network to map complex input-output relationships. Meanwhile, the DDRE integrates prior knowledge from a well-trained model to estimate spatially variable blur information, allowing the router to map the learned degradation representation and assign weights to experts based on the degree of degradation and the size of the regions. Experimental results demonstrate that our DHNet outperforms state-of-the-art approaches.



## References

- [1] Monami Banerjee, Rudransh Chakraborty, Jose Bouza, and Baba C. Vemuri. Voltteranet: A higher order convolutional network with group equivariance for homogeneous manifolds. *IEEE Transactions on Pattern Analysis and Machine Intelligence*, 44(2):823–833, 2022. 3
- [2] Liangyu Chen, Xiaojie Chu, Xiangyu Zhang, and Jian Sun. Simple baselines for image restoration. *ECCV*, 2022. 1, 2, 3, 6, 7, 8
- [3] Wuyang Chen, Yan-Quan Zhou, Nan Du, Yanping Huang, James Laudon, Z. Chen, and Claire Cu. Lifelong language pretraining with distribution-specialized experts. In *International Conference on Machine Learning*, 2023. 3, 5, 1
- [4] Xiang Chen, Hao Li, Mingqiang Li, and Jinshan Pan. Learning a sparse transformer network for effective image deraining. In *Proceedings of the IEEE/CVF Conference on Computer Vision and Pattern Recognition (CVPR)*, pages 5896–5905, 2023. 3
- [5] Xiang Chen, Jinshan Pan, Jiyang Lu, Zhentao Fan, and Hao Li. Hybrid cnn-transformer feature fusion for single image deraining. *Proceedings of the AAAI Conference on Artificial Intelligence*, 37(1):378–386, 2023. 3
- [6] Yuning Cui, Wenqi Ren, Xiaochun Cao, and Alois Knoll. Focal network for image restoration. In *Proceedings of the IEEE/CVF International Conference on Computer Vision*, pages 13001–13011, 2023. 2
- [7] Yuning Cui, Wenqi Ren, Sining Yang, Xiaochun Cao, and Alois Knoll. Irnext: Rethinking convolutional network design for image restoration. In *Proceedings of the 40th International Conference on Machine Learning*, 2023. 1, 2, 6
- [8] Yuning Cui, Yi Tao, Zhenshan Bing, Wenqi Ren, Xinwei Gao, Xiaochun Cao, Kai Huang, and Alois Knoll. Selective frequency network for image restoration. In *The Eleventh International Conference on Learning Representations*, 2023. 1, 6
- [9] Yuning Cui, Yi Tao, Wenqi Ren, and Alois Knoll. Dual-domain attention for image deblurring. *Proceedings of the AAAI Conference on Artificial Intelligence*, 37(1):479–487, 2023.
- [10] Yuning Cui, Wenqi Ren, Xiaochun Cao, and Alois Knoll. Image restoration via frequency selection. *IEEE Transactions on Pattern Analysis and Machine Intelligence*, 46(2): 1093–1108, 2024. 1, 2, 4, 6
- [11] J. Dong, J. Pan, Z. Yang, and J. Tang. Multi-scale residual low-pass filter network for image deblurring. In *2023 IEEE/CVF International Conference on Computer Vision (ICCV)*, pages 12311–12320, 2023. 3, 6, 4
- [12] Weisheng Dong, Lei Zhang, Guangming Shi, and Xiaolin Wu. Image deblurring and super-resolution by adaptive sparse domain selection and adaptive regularization. *IEEE Transactions on Image Processing*, 20(7):1838–1857, 2011. 2
- [13] Zhenxuan Fang, Fangfang Wu, Weisheng Dong, Xin Li, Jinjian Wu, and Guangming Shi. Self-supervised non-uniform kernel estimation with flow-based motion prior for blind image deblurring. In *Proceedings of the IEEE/CVF Conference on Computer Vision and Pattern Recognition (CVPR)*, pages 18105–18114, 2023. 6, 7, 8
- [14] William Fedus, Barret Zoph, and Noam Shazeer. Switch transformers: scaling to trillion parameter models with simple and efficient sparsity. *The Journal of Machine Learning Research*, 23(1), 2022. 3
- [15] Xin Feng, Haobo Ji, Wenjie Pei, Jinxing Li, Guangming Lu, and David Zhang. U2-former: Nested u-shaped transformer for image restoration via multi-view contrastive learning. *IEEE Transactions on Circuits and Systems for Video Technology*, pages 1–1, 2023. 1, 3
- [16] Hu Gao, Bowen Ma, Ying Zhang, Jingfan Yang, Jing Yang, and Depeng Dang. Learning enriched features via selective state spaces model for efficient image deblurring. In *Proceedings of the 32nd ACM International Conference on Multimedia*, page 710–718, 2024. 1, 6, 7, 4
- [17] Amirhosein Ghasemabadi, Muhammad Kamran Janjua, Mohammad Salameh, CHUNHUA ZHOU, Fengyu Sun, and Di Niu. Cascadedgaze: Efficiency in global context extraction for image restoration. *Transactions on Machine Learning Research*, 2024. 2
- [18] Hang Guo, Jinmin Li, Tao Dai, Zhihao Ouyang, Xudong Ren, and Shu-Tao Xia. Mambair: A simple baseline for image restoration with state-space model. *arXiv preprint arXiv:2402.15648*, 2024. 6, 7, 4
- [19] Robert A. Jacobs, Michael I. Jordan, Steven J. Nowlan, and Geoffrey E. Hinton. Adaptive mixtures of local experts. *Neural Computation*, 3(1):79–87, 1991. 3
- [20] Ali Karaali and Claudio Rosito Jung. Edge-based defocus blur estimation with adaptive scale selection. *IEEE Transactions on Image Processing*, 27(3):1126–1137, 2017. 1, 2
- [21] D. Kingma and J. Ba. Adam: A method for stochastic optimization. *Computer Science*, 2014. 6
- [22] Lingshun Kong, Jiangxin Dong, Jianjun Ge, Mingqiang Li, and Jinshan Pan. Efficient frequency domain-based transformers for high-quality image deblurring. In *Proceedings of the IEEE/CVF Conference on Computer Vision and Pattern Recognition*, pages 5886–5895, 2023. 1, 3, 7
- [23] Orest Kupyn, T. Martyniuk, Junru Wu, and Zhangyang Wang. Deblurgan-v2: Deblurring (orders-of-magnitude) faster and better. *2019 IEEE/CVF International Conference on Computer Vision (ICCV)*, pages 8877–8886, 2019. 7
- [24] Jingyun Liang, Jiezhong Cao, Guolei Sun, Kai Zhang, Luc Van Gool, and Radu Timofte. Swinir: Image restoration using swin transformer. *arXiv preprint arXiv:2108.10257*, 2021. 3
- [25] Hanzhou Liu, Binghan Li, Chengkai Liu, and Mi Lu. Deblurdinat: A lightweight and effective transformer for image deblurring, 2024. 3
- [26] I. Loshchilov and F. Hutter. Sgdr: Stochastic gradient descent with warm restarts. 2016. 6
- [27] Xintian Mao, Qingli Li, and Yan Wang. Adarevd: Adaptive patch exiting reversible decoder pushes the limit of image deblurring. In *Proceedings of the IEEE/CVF Conference on Computer Vision and Pattern Recognition (CVPR)*, pages 25681–25690, 2024. 2, 3, 4, 5, 6, 7, 1

- [28] Basil Mustafa, Carlos Riquelme Ruiz, Joan Puigcerver, Rodolphe Jenatton, and Neil Houlsby. Multimodal contrastive learning with LIMoe: the language-image mixture of experts. In *Advances in Neural Information Processing Systems*, 2022. 3
- [29] Seungjun Nah, Tae Hyun Kim, and Kyoung Mu Lee. Deep multi-scale convolutional neural network for dynamic scene deblurring. *2017 IEEE Conference on Computer Vision and Pattern Recognition (CVPR)*, pages 257–265, 2016. 2, 6, 7, 3, 4
- [30] Vaishnav Potlapalli, Syed Waqas Zamir, Salman Khan, and Fahad Shahbaz Khan. Promptir: Prompting for all-in-one blind image restoration. *Advances in Neural Information Processing Systems (NeurIPS)*, 2023. 1, 3
- [31] Jaesung Rim, Haeyun Lee, Jucheol Won, and Sunghyun Cho. Real-world blur dataset for learning and benchmarking deblurring algorithms. In *Proceedings of the European Conference on Computer Vision (ECCV)*, 2020. 6, 7, 3
- [32] Siddharth Roheda, Hamid Krim, and Bo Jiang. Volterra neural networks (vnns). *Journal of Machine Learning Research*, 25(182):1–29, 2024. 3, 5, 1
- [33] Siddharth Roheda, Amit Unde, and Loay Rashid. Mr-vnet: Media restoration using volterra networks. In *Proceedings of the IEEE/CVF Conference on Computer Vision and Pattern Recognition (CVPR)*, pages 6098–6107, 2024. 2, 3, 4, 5, 6, 7, 1
- [34] Carlos Riquelme Ruiz, Joan Puigcerver, Basil Mustafa, Maxim Neumann, Rodolphe Jenatton, André Susano Pinto, Daniel Keysers, and Neil Houlsby. Scaling vision with sparse mixture of experts. In *Advances in Neural Information Processing Systems*, 2021. 3
- [35] Ziyi Shen, Wenguan Wang, Xiankai Lu, Jianbing Shen, Haibin Ling, Tingfa Xu, and Ling Shao. Human-aware motion deblurring. *2019 IEEE/CVF International Conference on Computer Vision (ICCV)*, pages 5571–5580, 2019. 6, 7, 4
- [36] Fu-Jen Tsai, Yan-Tsung Peng, Yen-Yu Lin, Chung-Chi Tsai, and Chia-Wen Lin. Stripformer: Strip transformer for fast image deblurring. In *ECCV*, 2022. 3, 7
- [37] Vito Volterra. Theory of functionals and of integral and integro-differential equations. 2005. 3
- [38] Zhendong Wang, Xiaodong Cun, Jianmin Bao, Wengang Zhou, Jianzhuang Liu, and Houqiang Li. Uformer: A general u-shaped transformer for image restoration. In *Proceedings of the IEEE/CVF Conference on Computer Vision and Pattern Recognition (CVPR)*, pages 17683–17693, 2022. 3, 6
- [39] Mao Xintian, Liu Yiming, Liu Fengze, Li Qingli, Shen Wei, and Wang Yan. Intriguing findings of frequency selection for image deblurring. In *Proceedings of the 37th AAAI Conference on Artificial Intelligence*, 2023. 6, 7
- [40] Tian Ye, Sixiang Chen, Yun Liu, Erkang Chen, and Yuche Li. Towards efficient single image dehazing and desnowing. *ArXiv*, abs/2204.08899, 2022. 3
- [41] Jiazuo Yu, Yunzhi Zhuge, Lu Zhang, Ping Hu, Dong Wang, Huchuan Lu, and You He. Boosting continual learning of vision-language models via mixture-of-experts adapters. *2024 IEEE/CVF Conference on Computer Vision and Pattern Recognition (CVPR)*, pages 23219–23230, 2024. 3, 5, 1
- [42] Syed Waqas Zamir, Aditya Arora, Salman Khan, Munawar Hayat, Fahad Shahbaz Khan, Ming-Hsuan Yang, and Ling Shao. Multi-stage progressive image restoration. In *CVPR*, 2021. 1, 2, 6, 7, 4
- [43] Syed Waqas Zamir, Aditya Arora, Salman Khan, Munawar Hayat, Fahad Shahbaz Khan, and Ming-Hsuan Yang. Restormer: Efficient transformer for high-resolution image restoration. In *CVPR*, 2022. 1, 3, 6, 4
- [44] Syed Waqas Zamir, Aditya Arora, Salman Khan, Munawar Hayat, Fahad Shahbaz Khan, Ming-Hsuan Yang, and Ling Shao. Learning enriched features for fast image restoration and enhancement. *IEEE Transactions on Pattern Analysis and Machine Intelligence (TPAMI)*, 2022. 2
- [45] Xiaoqiang Zhou, Huaibo Huang, Zilei Wang, and Ran He. Ristra: Recursive image super-resolution transformer with relativistic assessment. *IEEE Transactions on Multimedia*, pages 1–12, 2024. 3
- [46] Georgios Zoumpourlis, Alexandros Doumanoglou, Nicholas Vretos, and Petros Daras. Non-linear convolution filters for cnn-based learning. In *2017 IEEE International Conference on Computer Vision (ICCV)*, pages 4771–4779, 2017. 3

# Towards Differential Handling of Various Blur Regions for Accurate Image Deblurring

## Supplementary Material

### 6. Overview

The supplementary material is composed of:

Motivation Analysis: Sec.7

More Proof for VBlock: Sec.8

Loss Function: Sec.9

More Ablation Studies: Sec.10

Additional Visual Results: Sec.11

### 7. Motivation Analysis

Although existing image deblurring methods [22, 33] have demonstrated strong performance, they fail to account for the varying degrees of degradation across different regions. As shown in Figure 9, the blur intensity differs across regions of the image. Additionally, Figure 10 highlights that larger blurred regions are more challenging to recover. To address the first issue, AdaRevD [27] introduces a classifier to assess the degradation degree of image patches. However, AdaRevD [27] relies on a limited set of predefined categories and a fixed blur patch size, which restricts its ability to effectively adapt to different degradation degrees across varying patch sizes. This limitation prevents it from adequately solving the second problem.

In this paper, we propose the degradation degree recognition expert (DDRE) module which enables the model to adaptively handle varying degrees of degradation in blurred regions. Unlike conventional mixture of experts methods [3, 41], where each router selects only one expert and a subset of experts for processing, our DDRE first integrates prior knowledge from a well-trained model to estimate spatially varying blur information. It then utilizes all available routing paths, dynamically assigning weights to each expert along every path. As shown in Table 6, each expert is configured with convolutions of varying receptive field sizes, allowing it to identify degraded regions at different scales. To further validate the effectiveness of the DDRE module, we visualize the feature map in Figure 8. Compared to the initial feature map, the DDRE module recovers images with clearer details, such as the phone number on the white car advertisement. Moreover, the different routers exhibit varying abilities to handle blur degradation, demonstrating that our method can adaptively address blur with different degrees of degradation.

Table 6. The configuration of each expert.

Expert	Configuration
(1)	1x1 depthwise separable convolution
(2)	3x3 depthwise separable convolution
(3)	5x5 depthwise separable convolution
(4)	7x7 depthwise separable convolution
(5)	9x9 depthwise separable convolution

### 8. More Proof for VBlock

Our theoretical proof ideas are borrowed from VNNs [32]. A Volterra kernel with  $L$  terms, it can be expressed as:

$$y_k = h_0 + \sum_{d=1}^n \sum_{r_1=0}^{L-1} \dots \sum_{r_d=0}^{L-1} h_d(r_1 \dots r_d) \prod_{j=1}^d x(k - r_j) \quad (13)$$

where  $d$  represents the order,  $n$  is the maximum number of  $b$ , and  $r_d$  denotes the memory delay.

For image data, the feature value at location  $[x_1, x_2]$  in feature map  $F$  is computed using a 2D version of the Volterra kernel, as expressed:

$$\begin{aligned} F_z \begin{bmatrix} x_1 \\ x_2 \end{bmatrix} &= V_z(F_{z-1} \begin{bmatrix} x_1 - p_1 : x_1 + p_1 \\ x_2 - p_2 : x_2 + p_2 \end{bmatrix}) \\ &= \sum_{r_{11}, r_{21}} h_1 \begin{bmatrix} r_{11} \\ r_{21} \end{bmatrix} x \begin{bmatrix} x_1 - r_{11} \\ x_2 - r_{21} \end{bmatrix} \\ &+ \sum_{\substack{r_{11}, r_{21} \\ r_{12}, r_{22}}} h_2 \begin{bmatrix} r_{11} \\ r_{21} \end{bmatrix} \begin{bmatrix} r_{12} \\ r_{22} \end{bmatrix} x \begin{bmatrix} x_1 - r_{11} \\ x_2 - r_{21} \end{bmatrix} x \begin{bmatrix} x_1 - r_{12} \\ x_2 - r_{22} \end{bmatrix} \\ &+ \dots \end{aligned} \quad (14)$$

where  $V_z$  denotes the  $z_{th}$  layer of the Volterra kernel,  $r_{1i} \in [-p_1, p_1]$  and  $r_{2i} \in [-p_2, p_2]$  represent spatial translations in the horizontal and vertical directions, respectively. The complexity of a  $n_{-th}$  order Volterra kernel is computed as:

$$\sum_{d=1}^n (L[2p_1 + 1][2p_2 + 1])^d \quad (15)$$

The Volterra kernel described earlier is significantly more expressive because it captures higher-order relationships among inputs. However, its computation requires iterated integrals and does not have an efficient GPU implementation. To overcome this limitation, we approximate higher-order behavior by utilizing a convex combination of the first-order and second-order terms of the Volterra kernel.

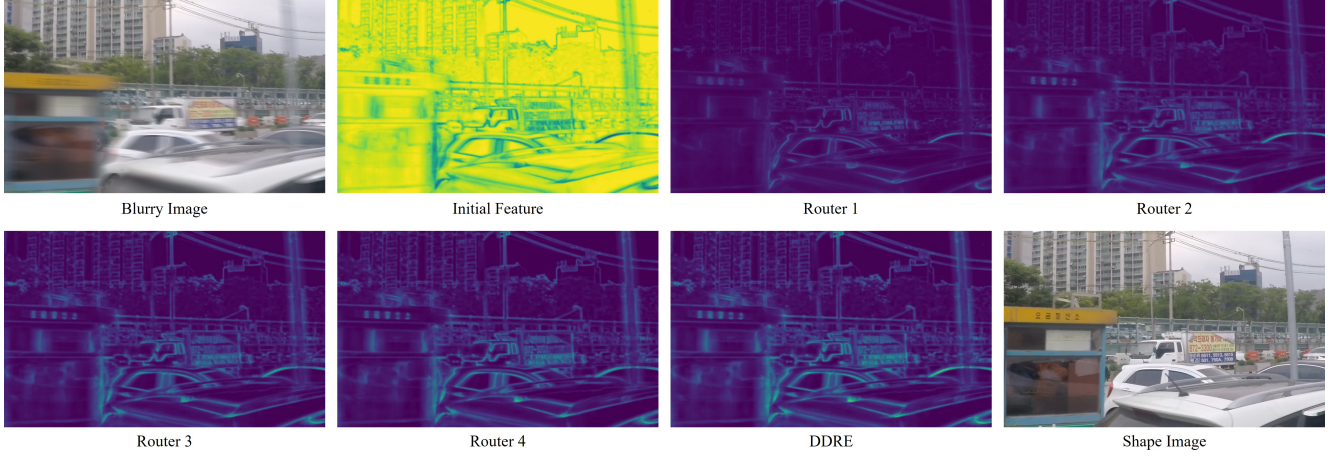


Figure 8. The internal features of DDRE.

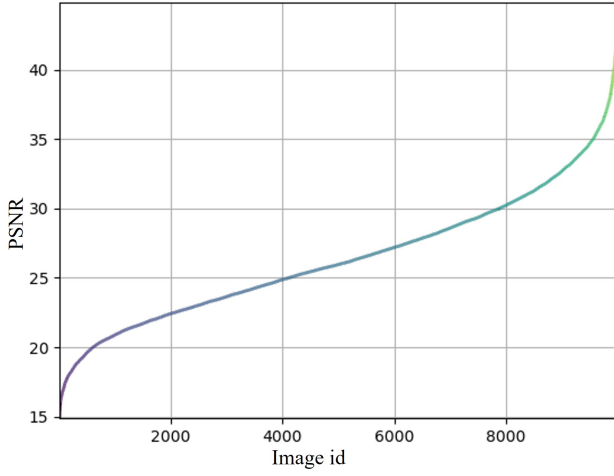


Figure 9. The ranked PSNR curve of the different blur region from GoPro [29] test set.

**Theorem 3.** A cascade of second-order Volterra kernels can approximate the higher-order behavior.

**Proof.** The second-order Volterra kernel can be formulated as:

$$\sigma_{v2}(x) = h_0 + h_1x + h_2x^2 \quad (16)$$

After feeding the output of the second-order Volterra kernel  $\sigma_{v2}(\cdot)$  back into another second-order Volterra kernel, we obtain an output that reaches up to the fourth order:

$$\begin{aligned} \sigma_{v2}(\sigma_{v2}(x)) &= \sigma_{v2}(h_0 + h_1x + h_2x^2) \\ &= h'_0 + h'_1x + h'_2x^2 + h'_3x^3 + h'_4x^4 \end{aligned} \quad (17)$$

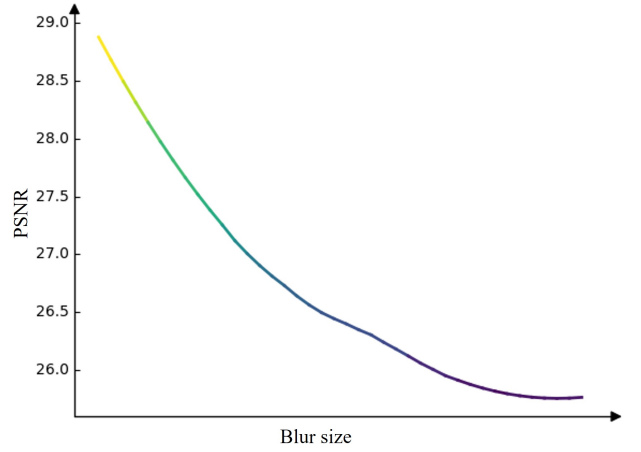


Figure 10. The PSNR curve of the different blur size from Go-Pro [29] test set.

where:

$$\begin{aligned} h'_0 &= h_0 + h_0^2h_2 \\ h'_1 &= h_0h_1 + 2h_0h_1h_2 \\ h'_2 &= h_1^2h_2 + h_1^2 \\ h'_3 &= 2h_1h_2h_2^2 + h_1h_2 \\ h'_4 &= h_2^3 \end{aligned} \quad (18)$$

Therefore, we can utilize  $K$  instances of the second-order Volterra kernel to implement an  $n_{-th}$  order Volterra kernel, where  $n = 2^{2^{K-1}}$ .

**Theorem 4.** The complexity of an  $n_{-th}$  order Volterra kernel, implemented using cascaded second-order Volterra kernels, is calculated as follows:



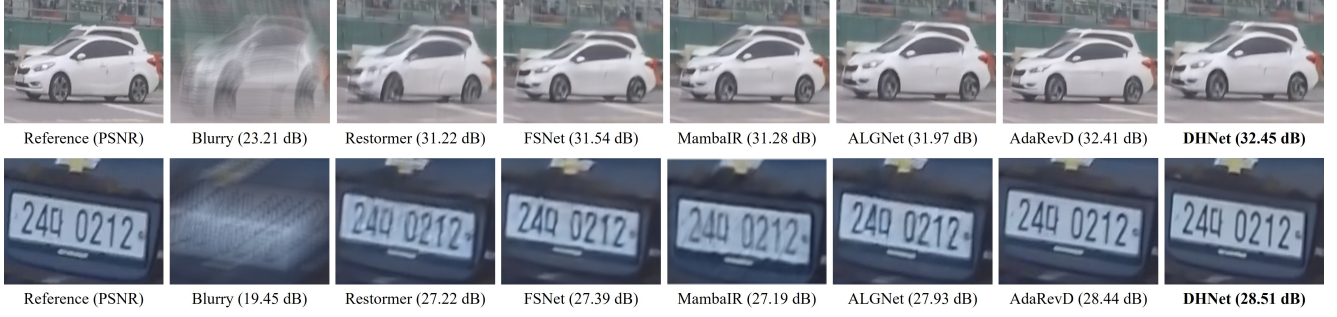


Figure 11. Comparison of image motion deblurring on the GoPro dataset [29].



Figure 12. Comparison of image motion deblurring on the RealBlur dataset [31].

$$\sum_{k=1}^K [(L_k[2p_{1k} + 1][2p_{2k} + 1]) + (L_k[2p_{1k} + 1][2p_{2k} + 1])^2] \quad (19)$$

**Proof.** It follows from Eq. 15 that, for a second-order Volterra kernel, the number of parameters required is  $[(L_k[2p_1 + 1][2p_2 + 1]) + (L_k[2p_1 + 1][2p_2 + 1])^2]$ . When we utilize  $K$  times of the second-order Volterra kernel to implement an  $n$ -th order Volterra kernel, it will lead to Eq. 19, which is significantly lower than Eq. 15.

The first order Volterra kernel is similar to the convolutional layer in the conventional CNNs. The second order kernel may be approximated as the concept of separable kernels as :

$$W_d^2 = \sum_{q=1}^Q W_d^{2aq} \otimes W_d^{2bq} \quad (20)$$

where  $Q$  represents the desired rank of approximation,  $W_d^2 \in \mathbb{R}^{(2p_1+1) \times (2p_2+1) \times (2p_1+1) \times (2p_2+1)}$ ,  $W_d^{2aq} \in \mathbb{R}^{(2p_1+1) \times (2p_2+1) \times 1}$  and  $W_d^{2bq} \in \mathbb{R}^{1 \times (2p_1+1) \times (2p_2+1)}$ . A larger  $Q$  will provide a better approximation of the second order kernel. This is easier to implement with a convolutional library in the first place. Secondly, the complexity is

reduced from Eq. 19 to:

$$\sum_{k=1}^K [(L_k[2p_{1k} + 1][2p_{2k} + 1]) + 2Q(L_k[2p_{1k} + 1][2p_{2k} + 1])] \quad (21)$$

Therefore, we can adjust the value of  $Q$  to strike a balance between performance and acceptable computational complexity. We also illustrate the impact of different  $Q$  values on the model in the ablation experiments presented in the main text.

## 9. Loss Function

To optimize the proposed network DHNet by minimizing the following loss function:

$$\begin{aligned} L &= L_c(\hat{I}, \bar{I}) + \delta L_e(\hat{I}, \bar{I}) + \lambda L_f(\hat{I}, \bar{I}) \\ L_c &= \sqrt{\|\hat{I} - \bar{I}\|^2 + \epsilon^2} \\ L_e &= \sqrt{\|\Delta \hat{I} - \Delta \bar{I}\|^2 + \epsilon^2} \\ L_f &= \|\mathcal{F}(\hat{I}) - \mathcal{F}(\bar{I})\|_1 \end{aligned} \quad (22)$$

where  $\bar{I}$  denotes the target images and  $L_c$  is the Charbonnier loss with constant  $\epsilon = 0.001$ .  $L_e$  is the edge loss, where  $\Delta$  represents the Laplacian operator.  $L_f$  denotes the frequency domains loss, and  $\mathcal{F}$  represents fast Fourier transform. To



Figure 13. Comparison of image motion deblurring on the HIDE dataset [35] among MRLPFNet [11], AdaRevD [27], Restormer [43], FSNet [10], MambaIR [18], ALGNet [16], and our DHNet.

Table 7. Results of alternatives to VBlock.

Net	MR-VNN [33]	VBlock	PSNR	$\Delta$ PSNR
(a)	✓		34.51	-
(b)		✓	34.75	+0.24

control the relative importance of loss terms, we set the parameters  $\lambda = 0.1$  and  $\delta = 0.05$  as in [10, 42].

## 10. More Ablation Studies

We provide more ablation studies on the GoPro dataset [29].

### 10.1. VBlock vs. MR-VNet [33]

Unlike MR-VNet [33], which treats the Volterra filter as a complete block, our VBlock incorporates it as part of a block. The VBlock first captures local features using LN, 1x1, and 3x3 convolutions before entering the Volterra filter, and then applies two 3x3 convolutions for each order branch. Additionally, by fusing the first- and second-order components and including a residual connection for the pre-order, our VBlock effectively avoids the issues of local feature loss.

To validate the advantage of our VBlock over MR-VNet [33], we replace our VBlock with MR-VNet and present the results in Table 1. When replaced, the performance drops by 0.24 dB, demonstrating the superior performance of our VBlock. Additionally, MR-VNet [33] is prone to gradient collapse during practical training.

### 10.2. Resource Efficient

We evaluate the model complexity of our proposed approach and other state-of-the-art methods in terms of running time and MACs. As shown in Table 8, our method achieves the lowest MACs value while delivering competitive performance in terms of running time.

Table 8. The evaluation of model computational complexity.

Method	Time(s)	MACs(G)	PSNR $\uparrow$	SSIM $\uparrow$
MPRNet [42]	1.148	777	32.66	0.959
Restormer [43]	1.218	140	32.92	0.961
FSNet [10]	<u>0.362</u>	111	33.29	0.963
MambaIR [18]	0.743	439	33.21	0.962
MR-VNet [33]	0.388	<u>96</u>	34.04	0.969
AdaRevD-L [27]	0.761	460	<u>34.60</u>	<u>0.972</u>
<b>DHNet(Ours)</b>	<b>0.256</b>	<b>32</b>	33.28	0.964
<b>DHNet-B(Ours)</b>	0.499	111	<b>34.75</b>	<b>0.973</b>

## 11. Additional Visual Results

In this section, we present additional visual results alongside state-of-the-art methods to highlight the effectiveness of our proposed approach, as shown in Figures 11, 13, 12. It is clear that our model produces more visually appealing outputs for both synthetic and real-world motion deblurring compared to other methods.